AIP | Journal of Applied Physics

Mechanical deformations of boron nitride nanotubes in crossed junctions

Yadong Zhao, Xiaoming Chen, Cheol Park, Catharine C. Fay, Stanislaw Stupkiewicz, and Changhong Ke

Citation: Journal of Applied Physics **115**, 164305 (2014); doi: 10.1063/1.4872238
View online: http://dx.doi.org/10.1063/1.4872238
View Table of Contents: http://scitation.aip.org/content/aip/journal/jap/115/16?ver=pdfcov
Published by the AIP Publishing

Mechanical deformations of boron nitride nanotubes in crossed junctions

Yadong Zhao,[1,a)] Xiaoming Chen,[1,a)] Cheol Park,[2,3] Catharine C. Fay,[2] Stanislaw Stupkiewicz,[4] and Changhong Ke[1,b)]
[1]*Department of Mechanical Engineering, State University of New York at Binghamton, Binghamton, New York 13902, USA*
[2]*NASA Langley Research Center, Hampton, Virginia 23681, USA*
[3]*Department of Mechanical and Aerospace Engineering, University of Virginia, Charlottesville, Virginia 22904, USA*
[4]*Institute of Fundamental Technological Research, Warsaw, Poland*

(Received 27 January 2014; accepted 11 April 2014; published online 23 April 2014)

We present a study of the mechanical deformations of boron nitride nanotubes (BNNTs) in crossed junctions. The structure and deformation of the crossed tubes in the junction are characterized by using atomic force microscopy. Our results show that the total tube heights are reduced by 20%–33% at the crossed junctions formed by double-walled BNNTs with outer diameters in the range of 2.21–4.67 nm. The measured tube height reduction is found to be in a nearly linear relationship with the summation of the outer diameters of the two tubes forming the junction. The contact force between the two tubes in the junction is estimated based on contact mechanics theories and found to be within the range of 4.2–7.6 nN. The Young's modulus of BNNTs and their binding strengths with the substrate are quantified, based on the deformation profile of the upper tube in the junction, and are found to be 1.07 ± 0.11 TPa and 0.18–0.29 nJ/m, respectively. Finally, we perform finite element simulations on the mechanical deformations of the crossed BNNT junctions. The numerical simulation results are consistent with both the experimental measurements and the analytical analysis. The results reported in this paper contribute to a better understanding of the structural and mechanical properties of BNNTs and to the pursuit of their applications. © *2014 AIP Publishing LLC*. [http://dx.doi.org/10.1063/1.4872238]

I. INTRODUCTION

Boron nitride nanotubes (BNNTs)[1,2] are a type of one-dimensional nanostructure, and are composed of partially ionic B-N bonding networks with boron and nitrogen atoms being positioned alternatively in a hexagonal honeycomb architecture. From a structural point of view, BNNTs are quite similar to their pure carbon counterparts, carbon nanotubes (CNTs). Research has revealed that BNNTs possess extraordinary physical properties, many of which are comparable or even superior to CNTs. For instance, the Young's modulus and strength of BNNTs are found to be up to 1.3 TPa and 33 GPa,[3–10] respectively. The shear strength of BNNTs is also reported to be much higher than that of CNTs.[11] BNNTs have excellent thermal conductivity and stability. BNNTs are thermally stable at up to 800 °C in air,[12,13] compared with up to just 400 °C for CNTs.[14,15] Unlike the metallic or semiconductive properties of CNTs, BNNTs are excellent electrical insulators with a bandgap of about 5.5 eV.[1,16,17] BNNTs are promising for a number of applications, such as mechanical and thermal reinforcing additives for polymeric and ceramic nanocomposites,[18] protective shields/capsules,[19] electrical insulators and optoelectronics devices.[20]

In spite of the substantial advances on BNNT research since its discovery in 1994,[1] the knowledge of this material remains quite limited, in particular, when compared with the findings on CNTs that were first reported in 1991.[21] The main challenge in the research and applications of BNNTs is the difficulty in synthesizing high-quality samples. A recent breakthrough on manufacturing high-quality BNNTs using an innovative high-temperature pressure (HTP) (also called pressured vapor/condenser (PVC)) method[22] has provided opportunities to probe the intrinsic physical properties of this material. The HTP-synthesized BNNTs are reported to be highly crystalline, very long (up to at least a few hundred microns), and of small diameters. Our recent studies on the radial deformability of HTP-synthesized BNNTs using an atomic force microscopy (AFM)–based compression testing technique characterized the effective radial modulus of tubes with just 1-4 tube walls.[23,24] It is worthy of mentioning here that the quantity "effective radial modulus" is not a pure material property because it is also strongly dependent on the geometry of the structure (e.g., the outer diameter and the number of walls for nanotubes). Our studies show that BNNTs possess a relatively lower radial rigidity than CNTs of the same outer diameters and tube wall numbers. The observed difference in radial deformability between BNNTs and CNTs was experimentally confirmed by a later study of engineering the transverse deformation in nanotubes using a nanomembrane-covering scheme.[25,26] The results consistently show that BNNTs deform more in their transverse directions than comparable CNTs under the covering of monolayer graphene oxide sheets. In our latest studies, the collision, dynamic frictional and fracture properties of HTP-synthesized BNNTs were characterized using an AFM-based

[a)]Y. Zhao and X. Chen contributed equally to this work.
[b)]Author to whom correspondence should be addressed. Electronic mail: cke@binghamton.edu. Fax: 1-607-777-4620.

nanomechanical scribing technique.[27,28] In the nanoscribing experiment, one tube that stays on a flat substrate was laterally scribed by a moving AFM probe tip. The tube deformed in the radial direction and eventually fractured as a result of the increasing normal compressive load and the lateral collision force that the AFM tip exerted. The normal compressive load and the corresponding lateral collision force that resulted in fracture of BNNTs were experimentally characterized, and the fracture strength of BNNTs was quantified using contact mechanics theories. Our studies report a fracture strength of 9.1–15.5 GPa for double-walled BNNTs (DW-BNNTs).

In this paper, we present a study of the mechanical deformations of BNNTs in crossed junctions. The crossed tube junction is made of one pair of BNNTs with one tube crossed over the other. The upper tube is pulled down by its adhesion force with the substrate, which exerts a compressive load on the lower tube at the position of the contact. Consequently, both the upper and the lower tubes experience radial deformations at the junction position, while bending deformations also occur in the upper tube. The measurements of the original undeformed configurations of these two tubes and their deformations at the tube junction, together with the knowledge of the tubes' radial rigidities, enable a quantification of the bending rigidity of the upper tube and its Young's modulus. It is noted that crossed nanotube junctions formed by CNTs were previously investigated by both experimental measurements and theoretical simulations.[29–31] Because transverse deformations in CNTs have a substantial influence on their bandgap structures,[32,33] the electronic transport behavior of the CNT junction could be dramatically different from the original properties of the CNTs forming the junction, thus providing intriguing electrical properties and potential for novel electronics applications.[34] Prominent influence of transverse deformations on electronic structures was also reported for BNNTs.[35,36] Therefore, understanding the mechanical deformations of BNNTs in crossed junctions is of importance to probe their local electronic properties in the deformed junction configuration and to pursue their potential applications.

In this study, we employ high resolution AFM imaging and nanomechanical testing techniques to characterize the structure and deformation of the tubes in the junction. The relationship between the mechanical deformations of the tubes in the junction and their original structural configurations and radial deformability is investigated in detail. The Young's modulus of BNNTs is quantified using analytical contact and structural mechanics models, and is found to be about 1.07 TPa and consistent with the theoretical and experimental data reported in the literature. In addition, the binding strength between BNNTs and substrates is quantified based on the deformation profile of the upper tube in the tube junction. To support the validity of our analytical analysis based on simplified continuum mechanics models, we perform finite element simulations on the mechanical deformations of the crossed BNNT junctions. The numerical simulation results are consistent with both our experimental measurements and analytical analysis. The results reported here are useful to better understand the structural and mechanical properties of BNNTs and in the pursuit of their applications.

II. RESULTS AND DISCUSSION

A. Sample preparation and atomic force microscopy measurements

The BNNTs employed in this study were synthesized using HTP methods.[22] Our prior studies have shown that a majority of the grown tubes are double-walled with outer diameters mostly in the range of 2–4 nm.[23] As-synthesized BNNTs, which were in the form of white cotton-like powders, were first dispersed in de-ionized water by means of ultrasonication with the aid of ionic surfactants.[23] The dispersed nanotubes were then deposited, by spin-coating, on fresh silicon substrates for AFM measurements or on transmission electron microscopy (TEM) copper grids for high resolution TEM (HRTEM) characterization.

All the AFM measurements presented in this paper were performed at room temperature inside a XE-70 AFM from Park Systems. The AFM is equipped with a closed-loop feedback control module and operates at a tapping mode. Silicon AFM probes (Model T190R from Vista Probe) with a nominal tip radius of 10 nm and a spring constant of 48 N/m were employed for the AFM measurements. It is noted that the tapping mode AFM was employed in this study for two purposes. First, in tapping mode imaging, the contact between an AFM tip and a nanotube is in the attractive regime of the van der Waals interaction. The gentle touching of the AFM tip with the nanotube surface helps obtain high resolution topography image of the nanotube, with little to no alteration to the nanotube's structural integrity or deformation. Second, the same AFM probe used for imaging can be used to identify the exact wall number in the tested tube through a nanotube-flattening technique,[37,38] which is discussed in detail later in this section.

Figure 1(a) shows a representative AFM image of one crossed BNNT junction. From the topography image, in particular, the inset zoom-in image of the junction area, it can be clearly seen that one tube crosses over the other tube on the substrate with a cross angle θ of 83.7°. Here, we define the cross angle as the acute angle formed by the two crossed tubes. To examine the cross-sectional height reduction of the crossed tubes at the position of the junction, we plot the cross-sectional profile of each tube at a position that is away from the junction as well as of the tube junction, which is shown in Figure 1(b). The dotted lines in Figure 1(a) mark the respective locations for the AFM topographic line profiles shown in Figure 1(b). Simplified deformation profiles of the upper and the lower tubes in the junction along the longitudinal axis of the upper tube are illustrated in Figure 1(c). The height of the upper tube in the junction, h_u, is measured to be 3.55 nm. The outer diameter of the upper tube, D_u, is calculated to be 3.21 nm by considering that $D_u = h_u - t$,[23,24] where $t = 0.34$ nm is the thickness of single-layer B-N sheets.[22] Similarly, the height (h_l) and the outer diameter (D_l) of the lower tube are measured to be 3.61 nm and 3.27 nm, respectively, based on the blue curve shown in Figure 1(b). The deviation error in the nanotube height and

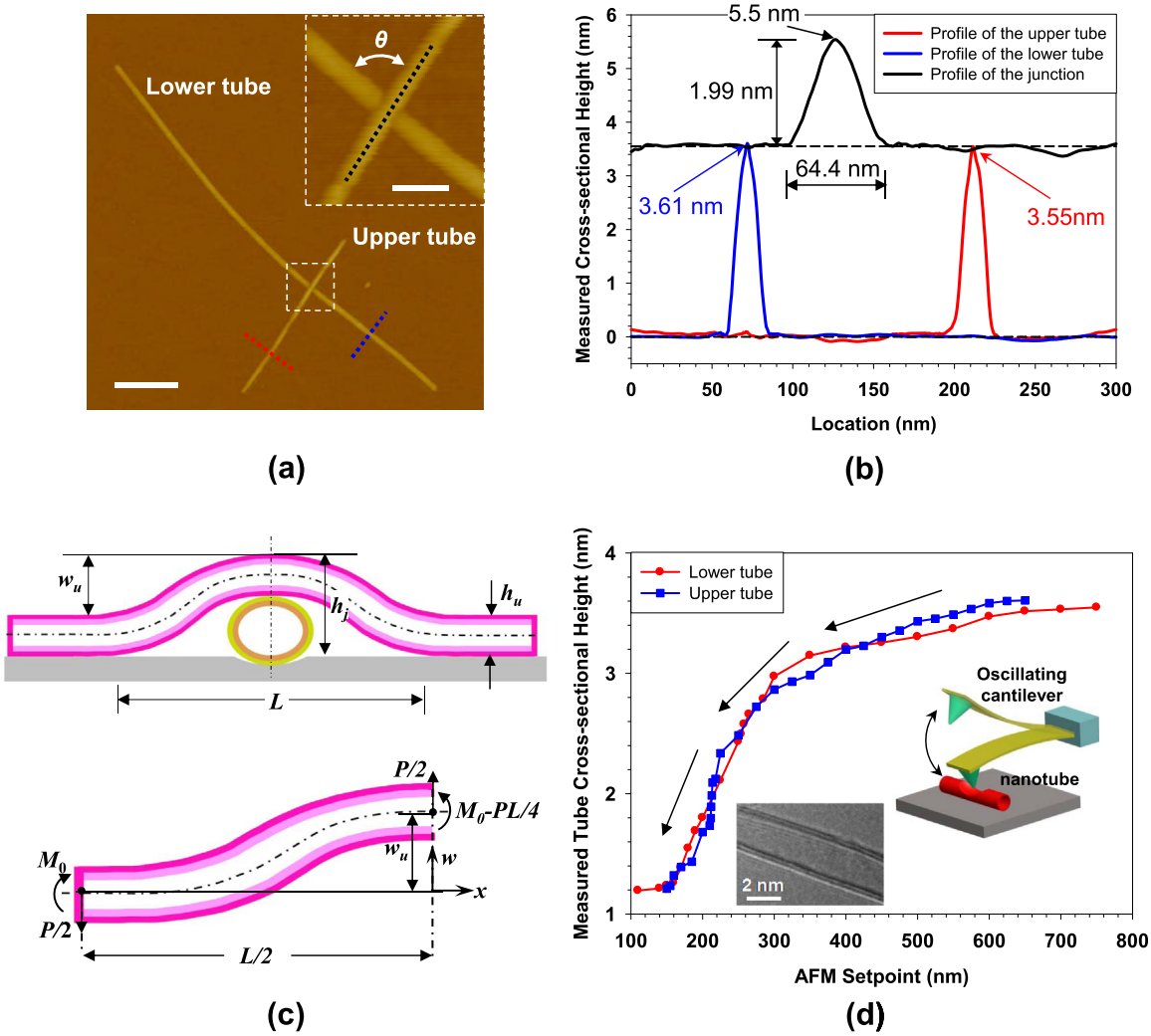

FIG. 1. (a) AFM image of a representative crossed BNNT junction (scale bar 200 nm). The inset shows a zoom-in view of the junction area (scale bar 50 nm). (b) AFM topographic profiles of the upper and the lower tubes and the tube junction along the, respectively, marked dotted lines in the AFM image shown in (a). (c) (*top*) Simplified deformation profiles of the upper and the lower tubes in the junction (cross-sectional view); (*bottom*) the free-body diagram of one-half of the upper tube. (d) AFM-based nanotube-flattening tests on both the upper and the lower tubes shown in (a). The inset drawing illustrates the approach of flattening a nanotube inside an AFM that operates at a tapping mode. The inset HRTEM image shows a double-walled BNNT with 3.1 nm in outer diameter.

diameter measurements is determined as the root mean square (rms) value of the measured AFM substrate scanning profile, and is calculated to be 0.09 nm for the two tubes in the junction shown in Figure 1(a). The total height of the crossed tubes at the junction, h_j, is measured to be 5.5 nm based on the black curve shown in Figure 1(b), compared to a value of 7.16 nm that is obtained through a simple summation of the original heights of these two tubes. Therefore, the cross-sectional height reduction of the two crossed tubes, Δh, is calculated to be 1.66 nm or about 23.2% of the sum of their original tube heights. We want to point out that the observed tube height reduction at the junction is not just due to the cross-sectional deformation of the two crossed tubes but also contributed by the deformation of the substrate. The presence of the lower tube essentially enforces a delamination of the upper tube from the substrate. The spanning width of the upper tube segment covering the top of the lower tube, L, which is defined as the distance between the two delamination fronts (see Figure 1(c)), is measured to be about 64.4 ± 1.3 nm from the AFM topography profile (i.e., the black curve shown in Figure 1(b)). The central deflection of the upper tube, w_u, is measured to be 1.99 nm.

In addition to the outer diameter, the number of walls in a nanotube is a prominent parameter in understanding its radial deformability.[23,24] Because the tested tubes stayed on flat substrates, they could not be directly visualized using commonly used HRTEM techniques. In this study, we employed an AFM-based nanotube-flattening technique[39] to quantify the number of tube walls inside the tubes in the crossed junction. In the nanotube-flattening test, a nanotube was compressed by an AFM probe at a position away from the junction point, as illustrated by the inset drawing in Figure 1(d). The AFM probe operated at a tapping mode with its tip being positioned right above the tube. The applied compressive load to the tube was adjusted by controlling the AFM setpoint, which is the oscillation amplitude of the AFM cantilever at the tip position. The cross-sectional height of the tube decreased with the increase of the compressive load, and eventually the tube collapsed under a sufficiently large load. This led to a flattened tube cross-section

whose height is nearly proportional to its number of tube walls. For instance, the cross-sectional height of a completely flattened single-walled BNNT is expected to be about 0.68 nm, while it is 1.36 nm for a DW-BNNT. The reason that we chose to perform the nanotube-flattening test by operating the AFM at a tapping mode, instead of at a contact mode that was reported in our prior studies,[22] is that such a test can be performed with the same probe that is used for topography imaging. Figure 1(d) shows the measured nanotube cross-sectional height as a function of the AFM setpoint for both the upper and the lower tubes in the crossed tube junction shown in Figure 1(a). For both tubes, the nanotube cross-sectional height decreased monotonously from their respective original heights down to about 1.2 nm. Considering the slight deformations of the AFM probe and the substrate during this flattening process,[22] both tubes are concluded to be double-walled based on their flattened cross-sectional heights. The inset HRTEM image in Figure 1(d) shows a typical DW-BNNT with an outer diameter of 3.1 nm. The HRTEM characterization of BNNTs was performed using a JEOL 2100F TEM.

We performed similar AFM imaging and flattening tests on a number of crossed BNNT junctions and identified 12 junctions that were composed of DW-BNNTs only with their outer diameters within the range of 2.21–4.67 nm. Table I lists the key experimentally measured and calculated data about the structure and deformation of the tubes in those junctions. The total tube cross-sectional height reduction at the junction is found to be in the range of 1.16–2.93 nm, or 20%–33% of the sum of the original tube heights. Figure 2(a) shows graphically the correlation between the total tube height reduction at the junction and the outer diameters of the upper and the lower nanotubes. Two scenarios are observed from the data presented in Figure 2(a). First of all, for the lower tubes with a similar diameter, the tube height reduction at the junction increases with the diameter of the upper tube. For instance, for the two pairs of data points enclosed in the red dashed line boxes shown in Figure 2(a), both of the lower tubes have an outer diameter of around 3.3 nm. The tube height reduction at the junction is found to increase from 1.44 to 1.65 nm, corresponding to an increase of the upper tube's diameter from 2.67 to 3.21 nm. Second, for the upper nanotubes with a similar diameter, the tube height reduction at the junction increases with the lower tube's diameter, which can be clearly observed from the two pairs of data points enclosed in the blue dashed line boxes shown in Figure 2(a). These results clearly indicate that the tube height reduction at the junction tends to be positively correlated with the outer diameters of both the upper and the lower tubes. We replot the same data shown in Figure 2(a) by changing the x-axis to be the sum of the outer diameters of the two tubes in the junction. The new plot, which is displayed in Figure 2(b), indeed shows the anticipated trend with a nearly linear relationship. The positive correlation between the tube height reduction and the outer diameters of the tubes can be qualitatively explained by the dependence of the radial rigidities of BNNTs on their outer diameters. Our recent studies show that the effective radial modulus of BNNTs increases with the number of tube walls, while decreasing with an increase in the outer diameter.[23] Therefore, it is reasonably expected that double-walled tubes of larger diameters are more apt to deform compared with those of smaller diameters. In Sec. II B 1, we provide quantitative analysis about the mechanical deformations of the tubes in the crossed junction.

B. Theoretical analysis

1. Contact force between the two crossed tubes

When a nanotube crosses over another nanotube on a flat substrate, the upper nanotube deforms and bends over the lower nanotube, resulting in a contact force between the two nanotubes. The contact force between the two crossed tubes is an important parameter to understanding their mechanical deformations in the junction. We estimate the contact force using a contact mechanics model by assuming that the junction is formed by two cylindrical bodies. In this model, we simplify the nanotube as a solid cylindrical elastic body and thus its radial rigidity can be represented by its effective radial modulus. Here, the effect of the van der Waals interaction between the tube and the substrate on the flattening of the tube cross-section is neglected and the

TABLE I. List of key experimentally measured and calculated parameters on the structure and deformation of BNNTs in the junction.

Sample	Upper tube outer diameter D_u (nm)	Lower tube outer diameter D_l (nm)	Spanning width of the upper tube L (nm)	Cross angle θ (deg)	Junction height h_j (nm)	Total tube height reduction at the junction Δh (nm)	Central deflection of the upper tube w_u (nm)
1	3.21 ± 0.09	3.27 ± 0.09	64.4 ± 1.3	83.7	5.50	1.66	1.99
2	3.60 ± 0.11	4.67 ± 0.11	78.8 ± 1.3	86.4	6.02	2.93	2.14
3	4.30 ± 0.10	3.87 ± 0.10	68.6 ± 1.4	38.8	6.02	2.83	1.40
4	2.87 ± 0.13	2.53 ± 0.13	50.4 ± 0.9	50.6	4.82	1.26	1.58
5	4.25 ± 0.14	3.99 ± 0.14	73.3 ± 1.5	39.3	6.34	2.59	1.82
6	3.48 ± 0.08	3.86 ± 0.08	71.0 ± 1.4	82.8	5.84	2.18	1.98
7	2.67 ± 0.07	3.27 ± 0.07	54.4 ± 1.1	54.0	5.18	1.44	2.16
8	2.49 ± 0.10	2.59 ± 0.10	49.0 ± 1.0	79.1	4.60	1.16	1.76
9	3.04 ± 0.12	3.55 ± 0.12	64.6 ± 1.1	80.6	5.48	1.78	2.06
10	3.95 ± 0.13	2.21 ± 0.13	54.4 ± 0.8	36.5	5.28	1.56	1.00
11	2.87 ± 0.09	3.68 ± 0.09	63.5 ± 1.0	63.1	5.46	1.77	2.29
12	2.99 ± 0.07	4.28 ± 0.07	64.6 ± 1.1	66.7	5.71	2.24	2.35

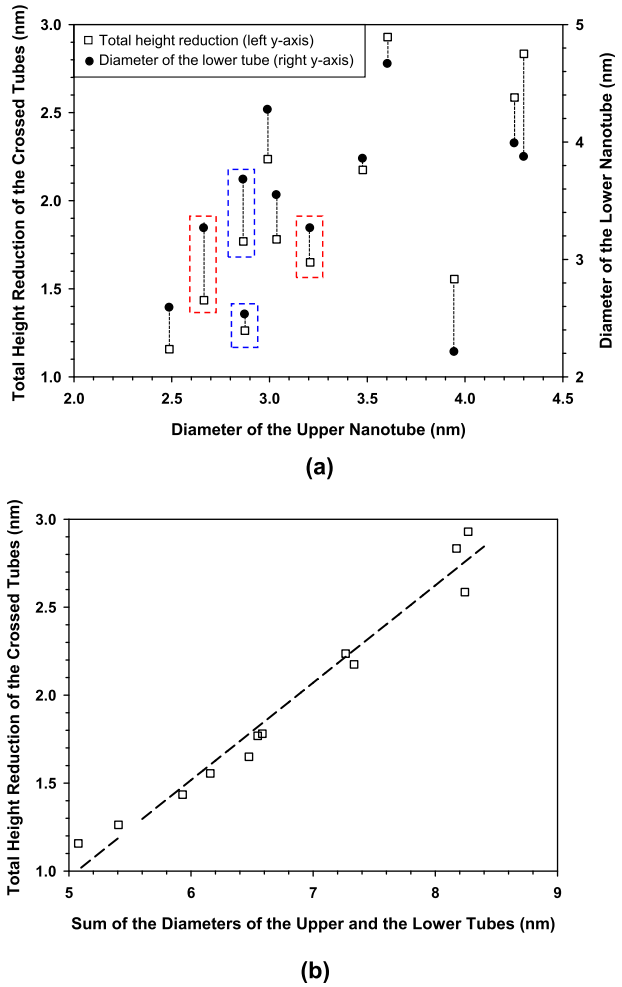

FIG. 2. (a) The total cross-sectional height reduction of the crossed tubes at the junction (left *y*-axis, empty-square). The *x*-axis labels the outer diameter of the upper BNNT in the junction. The right *y*-axis labels the outer diameter of the lower BNNT in the junction (solid-circle). The vertical dotted lines associate the data points measured on the same tube junctions. All the data presented are for tubes that are identified as double-walled BNNTs. (b) The dependence of the measured total cross-sectional height reduction of the crossed tubes at the junction on the sum of the outer diameters of the upper and the lower tubes in the junction.

original nanotube is assumed to undertake a circular cross-section.[40] The Hertzian contact between two crossed cylindrical bodies has an elliptical contact interface. The measured tube height reduction at the junction (denoted as Δh) is essentially equal to the combined nanotubes-substrate deformation, and is approximated by[24,41]

$$\Delta h = 2K(e)\left[\frac{3P}{4}k_1\right]^{2/3}\left[\left(\frac{\Phi\cdot e^2}{2(K(e)-E(e))}\right)\right]^{1/3} + \left[\frac{3P}{4\sqrt{D_l}}k_2\right]^{2/3}, \quad (1)$$

where $k_1 = \left(\frac{1-\nu_{nt}^2}{\pi E_u^{rad}} + \frac{1-\nu_{nt}^2}{\pi E_l^{rad}}\right)$ and $k_2 = \left(\frac{1-\nu_{sub}^2}{E_{sub}} + \frac{1-\nu_{nt}^2}{E_l^{rad}}\right)$. The first term on the right side of Eq. (1) represents the cross-sectional deformation in the two crossed tubes, while the second term represents the deformation in the lower nanotube and the substrate. P is the contact force between the two tubes that is simplified as a concentrated force. E_u^{rad} and E_l^{rad} are the effective radial moduli of the upper and the lower nanotubes, respectively. Recent studies show that the effective radial elastic modulus of DW-BNNTs (denoted as E^{rad} in general)[23] can be reasonably approximated as a simple power function of the tube's outer diameter (denoted as D in general), given by $E^{rad} = 241.3D^{-3.295}$ in which E^{rad} and D are in units of GPa and nm, respectively.[26] E_{sub} is the Young's modulus of the substrate, which is considered to be native silicon oxide with a Young's modulus of 74 GPa.[24] $\nu_{nt} = 0.2$ and $\nu_{sub} = 0.16$ (Ref. 24) are the Poisson's ratios of BNNTs and the substrate material, respectively. e is the eccentricity of the elliptical-shape contact between the two crossed tubes. $K(e) = \int_0^{\pi/2}(1-e^2\sin^2\lambda)^{-1/2}d\lambda$ and $E(e) = \int_0^{\pi/2}(1-e^2\sin^2\lambda)^{1/2}d\lambda$ are the complete elliptic integrals of the first and the second kinds, respectively. Φ is a parameter about the contact geometric shape of the two crossed nanotubes, which can be obtained from solving the following relationship:[41] $(2\Phi - 1/D_u - 1/D_l)^2 = (1/D_u)^2 + (1/D_l)^2 + (2\cos 2\theta)/(D_u D_l)$. The contact force P between the two crossed tubes can be obtained numerically from Eq. (1), based on the measured tube height reduction at the junction that is presented in Figure 2(a) and also listed in Table I. Figure 3(a) shows the calculated contact force P for all the 12 measured tube junctions, which is found to be in the range of 4.2–7.6 nN. Just for a reference purpose, Hertel *et al.* reported a contact force of about 5 nN between two crossed (10,10) single-walled CNTs on a graphite surface based on both continuum and molecular mechanics simulations.[40]

2. Young's modulus of BNNTs

In this section, we provide an analysis of the Young's modulus of BNNTs based on the deformation profiles of the tubes in the crossed junction and the contact force predicted in the Sec. II B 1. The Young's modulus of a nanotube defines its longitudinal (tensile) stress-strain relationship and is used to describe its flexural or bending rigidity. Here, we focus on the deformation of the upper tube in the junction and assume that it is a centrally loaded cylindrical beam with two fixed ends. From the junction formation process where the upper tube falls freely on top of the bottom tube, we reasonably assume that the deformation profile of the upper tube is governed by its bending deformation[30] and that the stretching effect in the upper tube should be quite minimal; thus is neglected here. The maximum deflection of the upper nanotube due to pure bending (w_u) occurs in the tube segment that covers the top of the lower tube (see Figure 1(c)) and is measured from the recorded topography profile of the upper tube in the junction. It is noted that w_u can be also approximated as the difference of the measured junction height and the original cross-sectional height of the upper tube, i.e., $w_u \approx h_j - h_u$. Based on beam theory,[42] $w_u = \frac{PL^3}{192EI}$, in which E is the Young's modulus of BNNTs and $I = \frac{\pi}{64}\left[D_u^4 - (D_u - 2t)^4\right]$ is the moment of inertia of the upper tube in the junction. Figure 3(b) shows the calculated Young's modulus of the BNNTs in the measured crossed

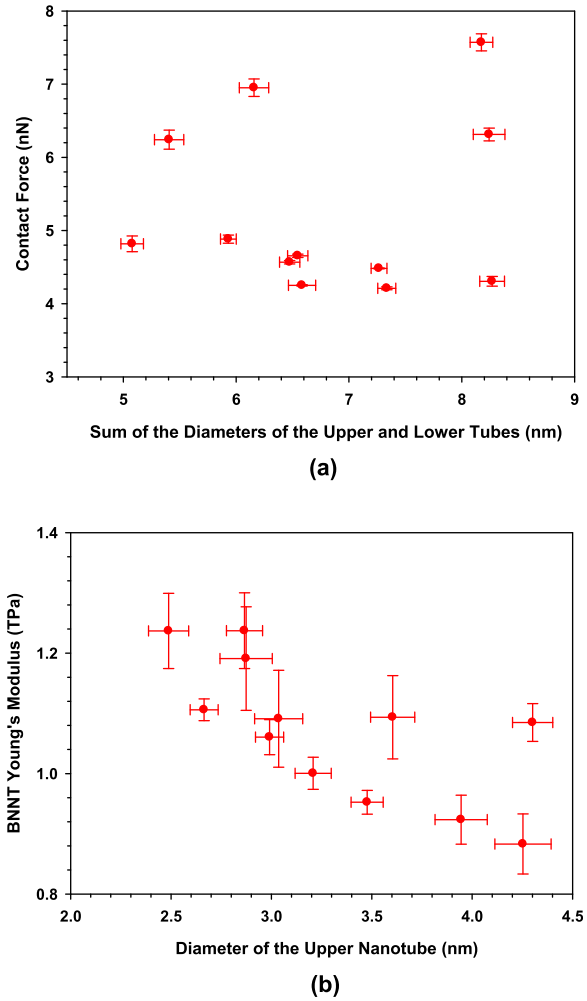

FIG. 3. (a) The dependence of the predicted contact force between the two crossed BNNTs in the junction on the sum of the outer diameters of the two crossed nanotubes. The horizontal error bar indicates the deviation in the measured nanotube's outer diameter. The vertical error bar indicates the deviation in the calculated contact force. (b) The calculated Young's modulus of BNNTs.

tube junctions. The average BNNT Young's modulus together with the corresponding root-mean-square (rms) deviation is found to be 1.07 ± 0.11 TPa. Previously, the Young's modulus of BNNTs has been theoretically predicated to be around 900 MPa by using tight-binding (TB) methods,[6] or to be 1.0–1.2 TPa by using the Tersoff–Brenner potential.[43] The reported experimental values for the Young's modulus of BNNTs are in the range of 0.7–1.3 TPa.[3,4,8] Therefore, the Young's modulus of BNNTs obtained in this study is consistent with all of those data reported in the literature and is quite close to the theoretically predicted intrinsic values for defect-free BNNTs.

3. Binding strength between BNNTs and substrates

The binding energy of the upper tube with the substrate can be estimated from its deformation profile. The forced delamination of the upper tube from the substrate due to the presence of the lower tube can be ascribed to a balanced competition between the bending moment and the adhesion energy at the delamination front. The bending moment in the upper tube at the delamination front is given by $M_0 = \frac{PL}{8}$. The adhesion energy per unit length or energy release rate at the delamination front is given by[25] $G = \frac{1}{2}\frac{M_0^2}{EI} = \frac{P^2L^2}{128EI}$. Figure 4(a) shows the calculated bending moment in the cross-section of the upper tube at the delamination front. Figure 4(b) shows the calculated binding energy between the upper tube and the substrate, which is found to be in the range of 0.18–0.29 nJ/m for tubes with outer diameters in the range of 2.49–4.30 nm. The adhesion of individual hexagonal-phase BNNTs with silicon substrates was previously investigated by Hsu *et al.* using lateral AFM-based nanomanipulation techniques.[44] A binding energy of 0.11–0.21 nJ/m was reported based on measurements of two tubes with diameters of 14 and 17 nm, respectively, which is quite close to our data on the BNNT-substrate binding energy.

C. Finite element simulations of crossed nanotube junctions

In addition to the theoretical analysis presented in Sec. II B, we perform numerical simulations on the mechanical deformations of the crossed BNNT junctions using finite element methods (FEM). The FEM simulation is conducted primarily to support our above-mentioned theoretical

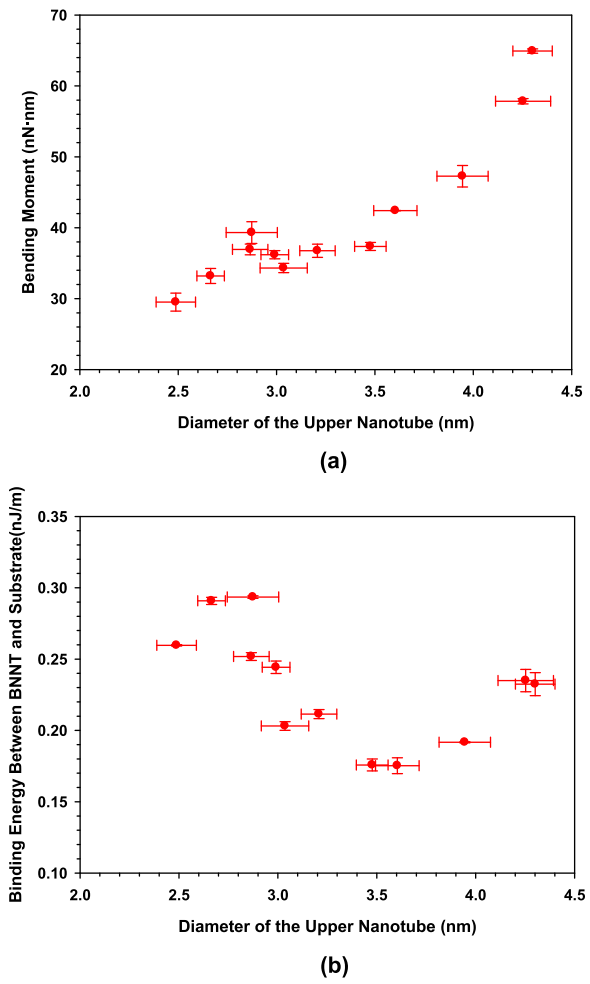

FIG. 4. (a) The calculated bending moment in the upper BNNT at the delamination front. (b) The calculated binding energy between the upper BNNT and the substrate.

analysis that is based on simplified models. It is noted that several assumptions are taken in our simplified models. For instance, the employed contact mechanics model, which is described by Eq. (1), was originally derived based on theories for small deformations, while the deformations of nanotubes in the crossed tube junction are expected to be in a finite deformation regime. The employed structural mechanics model does not fully take into account the effect of substantial local deformations at the tube junction on the bending deformation of the upper nanotube. The results from FEM simulations will be useful not only to validate results from the analytical analysis but also to better understand the experimental measurements.

For the FEM simulation, a three-dimensional (3D) continuum mechanics model is constructed for the crossed nanotube junction. The nanotubes are represented by elastic hollow cylinders, while the substrate is represented by an elastic block. Both the tube/tube and the tube/substrate contacts are assumed to be frictionless and adhesion-free. The FEM model enhances the analytical models presented in Sec. II B with three-dimensional effects in the finite deformation regime. The bodies of the tubes and the substrate are discretized using eight-node enhanced-strain solid elements to avoid so-called locking effects.[45] Material behaviors of the tube and the substrate are both governed by isotropic linear-elastic strain energies. To be consistent with the adopted definition of the tube's outer diameter in Sec. II A, the contact interaction is activated when the tube/tube or the tube/substrate separation reaches 0.34 nm. A robust contact formulation[46] based on a contact smoothing technique and augmented Lagrangian treatment of the impenetrability constraint is employed for the simulation. The same boundary conditions as those adopted in the analytical model presented in Sec. II B 1 are employed. In particular, the upper tube is clamped at both ends, and its axial force is enforced to be equal to zero.

Appropriate scaling of the Young's modulus and the tube wall thickness is an essential feature of the present FEM

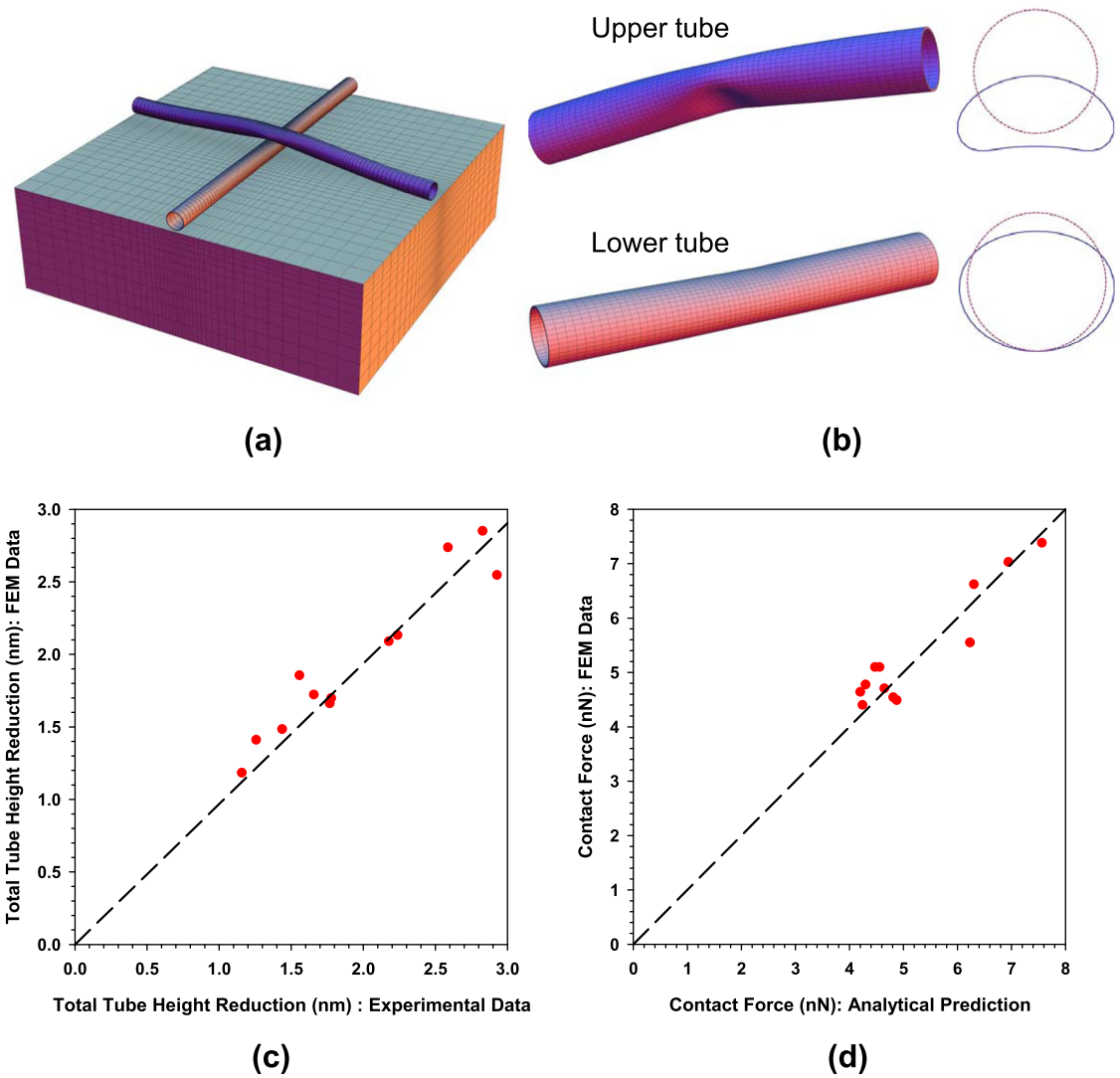

FIG. 5. (a), (b) The finite element simulation of the crossed tube junction shown in Figure 1(a). The global view of the junction is displayed in (a), while the local deformations of the upper and the lower tubes in the vicinity of the contact zone are displayed in (b). The solid blue curves shown next to the tube deformation snapshots in (b) are the respective central cross-sections of the deformed tubes, which are contrasted with their original undeformed shapes (dotted pink curves). (c) The comparison between the experimental measurements and the FEM results on the total tube height reduction at the junction. (d) The comparison between the analytical and the FEM results on the contact force between the two tubes in the junction. The dashed lines in (c) and (d) are the linear-fitting curves.

model. The transverse flexural stiffness is known to be a tube's property that is independent from its axial stiffness and overall bending rigidity.[31] Based on classical continuum mechanics theories, the flexural stiffness of a thin-plate is linearly proportional to its Young's modulus, while linearly proportional to the third order of its thickness. However, the transverse flexural stiffness of a nanotube wall member would be significantly over-predicted if the actual thickness of the tube wall was adopted in the continuum model. The thickness of the tube wall element shall be reduced by a factor $\alpha < 1$, while the tube's outer diameter (D_u) is kept unaltered. Meanwhile, its Young's modulus shall be increased by a factor of $1/\alpha$ such that the axial stiffness and the overall bending stiffness of the tube are approximately kept intact and not affected by the scaling. For instance, for single-walled CNTs, prior studies employed a reduced wall thickness of 0.066 nm in conjunction with a Young's modulus of 5.5 TPa,[31] which contrast with the actual nanotube wall thickness of 0.34 nm and Young's modulus of 1.06 TPa. Essentially, a scaling factor $\alpha = 0.2$ was employed for single-walled tubes. This scaling factor is also dependent on the number of walls in the tube. For our FEM simulations on double-walled BNNTs, we employ the average Young's modulus $E = 1.07$ TPa that is obtained in Sec. II B 2 as a before-scaling value of their Young's modulus. The scaling factor α with a value of 0.33 is identified to yield consistent results with the experimental measurements on the tube height reduction at the junction.

We perform FEM simulations for all the measured crossed tube junctions that are listed in Table I. The interaction between the two contacting tubes and their respective deformations are induced by means of specifying the boundary conditions to both the upper and the bottom tubes and conducting the simulations in a displacement-control manner. The upper tube is initially placed horizontally above the substrate, and is then controlled to fall on the bottom tube and the substrate, while the bottom tube is placed and remains at a standstill on the substrate. Figure 5(a) shows the deformation of the crossed tube junction and the corresponding deformed finite element meshes for the junction shown in Figure 1(a) (sample #1 in Table I). Detailed views of the local deformation in each tube in the vicinity of the contact zone are shown in Figure 5(b). The solid blue curves displayed next to the tube deformation snapshots are the respective central cross-sections of the deformed tubes, which are also contrasted with their original undeformed shapes (dotted purple curves). It can be clearly seen that the total tube height reduction at the junction is contributed mostly by the local deformation of the upper tube, which is quite substantial compared to its original shape. Figure 5(c) shows a comparison of the experimental measurements (x-axis) and the FEM results (y-axis) on the total tube height reduction at the position of the junction for all the 12 measured samples. The data clearly display a linear trend and the linear fitting curve (dashed line) has a slope of 0.985, which indicates a good agreement between the experimental measurements and the FEM simulation results. Figure 5(d) shows a comparison between the analytical and the FEM results on the contact force between the two tubes in the junction, and the linear fitting curve (dashed line) has a slope of 1.0. The good agreement indicated by the slope of the fitting line is largely anticipated because the average Young's modulus ($E = 1.07$ TPa) was employed in the FEM simulations. The small scattering of the data around the trend line shown in Figure 5(d) clearly supports the overall validity of the presented theoretical analysis in Sec. II B that is based on simplified continuum models. Such simple yet relatively accurate analytical models are quite useful in understanding the mechanical deformations of the tubes in the crossed junction.

III. CONCLUSION

In this paper, we investigate the mechanical deformation of BNNTs in crossed tube junctions using AFM in conjunction with contact and structural mechanics models and FEM simulations. Our study reveals that substantial transverse deformations occur to the crossed nanotubes in the vicinity of the junction region. The total tube height reduction at the junction is found to be almost linearly correlated with the sum of the outer diameters of the two tubes in the junction. The Young's modulus of BNNTs is estimated to be around 1.07 TPa based on the predicted contact force between the tubes in the junction and the deformation profile of the upper tube, and is quite close to the theoretically predicted values for defect-free BNNT structures. The results reported in this work are useful to better understand the structural and mechanical properties of BNNTs and in the pursuit of their structural applications. The observed substantial local deformation of BNNTs in the junction may also have implication on their electronic structures, thus their electrical properties and applications.

ACKNOWLEDGMENTS

This work was funded by U.S. Air Force Office of Scientific Research-Low Density Materials program under Grant Nos. FA9550-11-1-0042 and FA9550-10-1-0451. S.S. acknowledges the financial support of the National Science Center (NCN) in Poland under Grant No. 2011/01/B/ST8/07434. The authors thank Dr. In-tae Bae for his assistance with the TEM characterization. The TEM characterizations were performed using the facilities in the Analytical and Diagnostics Laboratory at Binghamton University's Small Scale Systems Integration and Packaging Center (S^3IP).

[1]A. Rubio, J. L. Corkill, and M. L. Cohen, Phys. Rev. B **49**, 5081 (1994).
[2]N. G. Chopra, R. J. Luyken, K. Cherrey, V. H. Crespi, M. L. Cohen, S. G. Louie, and A. Zettl, Science **269**, 966 (1995).
[3]X. Wei, M.-S. Wang, Y. Bando, and D. Golberg, Adv. Mater. **22**, 4895 (2010).
[4]N. G. Chopra and A. Zettl, Solid State Commun. **105**, 297 (1998).
[5]R. Arenal, M. S. Wang, Z. Xu, A. Loiseau, and D. Golberg, Nanotechnology **22**, 265704 (2011).
[6]E. Hernandez, C. Goze, P. Bernier, and A. Rubio, Phys. Rev. Lett. **80**, 4502 (1998).
[7]H. M. Ghassemi, C. H. Lee, Y. K. Yap, and R. S. Yassar, J. Appl. Phys. **108**, 024314 (2010).
[8]D.-M. Tang, C.-L. Ren, X. Wei, M.-S. Wang, C. Liu, Y. Bando, and D. Golberg, ACS Nano **5**, 7362 (2011).

[9]A. P. Suryavanshi, M.-F. Yu, J. Wen, C. Tang, and Y. Bando, Appl. Phys. Lett. **84**, 2527 (2004).
[10]D. Golberg, P. M. F. J. Costa, O. Lourie, M. Mitome, X. Bai, K. Kurashima, C. Zhi, C. Tang, and Y. Bando, Nano Lett. **7**, 2146 (2007).
[11]J. Garel, I. Leven, C. Zhi, K. S. Nagapriya, R. Popovitz-Biro, D. Golberg, Y. Bando, O. Hod, and E. Joselevich, Nano Lett. **12**, 6347 (2012).
[12]Y. Chen, J. Zou, S. J. Campbell, and G. Le Caer, Appl. Phys. Lett. **84**, 2430 (2004).
[13]D. Golberg, Y. Bando, K. Kurashima, and T. Sato, Scr. Mater. **44**, 1561 (2001).
[14]S. C. Tsang, P. J. F. Harris, and M. L. H. Green, Nature **362**, 520 (1993).
[15]P. M. Ajayan, T. W. Ebbesen, T. Ichihashi, S. Iijima, K. Tanigaki, and H. Hiura, Nature **362**, 522 (1993).
[16]C. H. Lee, M. Xie, V. Kayastha, J. S. Wang, and Y. K. Yap, Chem. Mater. **22**, 1782 (2010).
[17]X. Blase, A. Rubio, S. G. Louie, and M. L. Cohen, Europhys. Lett. **28**, 335 (1994).
[18]C. Y. Zhi, Y. Bando, T. Terao, C. C. Tang, H. Kuwahara, and D. Golberg, Adv. Funct. Mater. **19**, 1857 (2009).
[19]Y. B. Li, P. S. Dorozhkin, Y. Bando, and D. Golberg, Adv. Mater. **17**, 545 (2005).
[20]Z. G. Chen, J. Zou, G. Liu, F. Li, H. M. Cheng, T. Sekiguchi, M. Gu, X. D. Yao, L. Z. Wang, and G. Q. Lu, Appl. Phys. Lett. **94**, 023105 (2009).
[21]S. Iijima, Nature **354**, 56 (1991).
[22]M. W. Smith, K. C. Jordan, C. Park, J.-W. Kim, P. T. Lillehei, R. Crooks, and J. S. Harrison, Nanotechnology **20**, 505604 (2009).
[23]M. Zheng, C. Ke, I.-T. Bae, C. Park, M. W. Smith, and K. Jordan, Nanotechnology **23**, 095703 (2012).
[24]M. Zheng, X. Chen, I.-T. Bae, C. Ke, C. Park, M. W. Smith, and K. Jordan, Small **8**, 116 (2012).
[25]M. Zheng, L.-F. Zou, H. Wang, C. Park, and C. Ke, ACS Nano **6**, 1814 (2012).
[26]M. Zheng, L. Zou, H. Wang, C. Park, and C. Ke, J. Appl. Phys. **112**, 104318 (2012).
[27]M. Zheng, X. Chen, C. Park, C. C. Fay, N. M. Pugno, and C. Ke, Nanotechnology **24**, 505719 (2013).
[28]X. Chen, M. Zheng, C. Park, and C. Ke, Appl. Phys. Lett. **102**, 121912 (2013).
[29]T. Hertel, R. Martel, and P. Avouris, J. Phys. Chem. B **102**, 910 (1998).
[30]J. W. Janssen, S. G. Lemay, L. P. Kouwenhoven, and C. Dekker, Phys. Rev. B **65**, 115423 (2002).
[31]A. Pantano, D. M. Parks, and M. C. Boyce, J. Mech. Phys. Solids **52**, 789 (2004).
[32]A. P. M. Barboza, A. P. Gomes, B. S. Archanjo, P. T. Araujo, A. Jorio, A. S. Ferlauto, M. S. C. Mazzoni, H. Chacham, and B. R. A. Neves, Phys. Rev. Lett. **100**, 256804 (2008).
[33]B. Shan, G. W. Lakatos, S. Peng, and K. Cho, Appl. Phys. Lett. **87**, 173109 (2005).
[34]M. S. Fuhrer, J. Nygård, L. Shih, M. Forero, Y.-G. Yoon, M. S. C. Mazzoni, H. J. Choi, J. Ihm, S. G. Louie, A. Zettl, and P. L. McEuen, Science **288**, 494 (2000).
[35]X. D. Bai, D. Golberg, Y. Bando, C. Y. Zhi, C. C. Tang, M. Mitome, and K. Kurashima, Nano Lett. **7**, 632 (2007).
[36]H. M. Ghassemi, C. H. Lee, Y. K. Yap, and R. S. Yassar, Nanotechnology **23**, 105702 (2012).
[37]M.-F. Yu, T. Kowalewski, and R. S. Ruoff, Phys. Rev. Lett. **85**, 1456 (2000).
[38]J. Legleiter, Nanotechnology **20**, 245703 (2009).
[39]T. DeBorde, J. C. Joiner, M. R. Leyden, and E. D. Minot, Nano Lett. **8**, 3568 (2008).
[40]T. Hertel, R. E. Walkup, and P. Avouris, Phys. Rev. B **58**, 13870 (1998).
[41]M. J. Puttock and E. G. Thwaite, "Elastic compression of spheres and cylinders at point and line contact," Commonwealth Scientific and Industrial Research Organization, Melbourne, Australia, 1969.
[42]S. P. Timoshenko and J. N. Goodier, *Theory of Elasticity*, 3rd ed. (Mcgraw-Hill, 1970).
[43]V. Verma, V. K. Jindal, and K. Dharamvir, Nanotechnology **18**, 435711 (2007).
[44]J. H. Hsu and S. H. Chang, Appl. Surf. Sci. **256**, 1769 (2010).
[45]J. Korelc, U. Šolinc, and P. Wriggers, Comput. Mech. **46**, 641 (2010).
[46]J. Lengiewicz, J. Korelc, and S. Stupkiewicz, Int. J. Numer. Methods Eng. **85**, 1252 (2011).